Environmental Pollution 255 (2019) 113175

Contents lists available at ScienceDirect

Environmental Pollution

journal homepage: www.elsevier.com/locate/envpol

Characterization of laboratory and real driving emissions of individual Euro 6 light-duty vehicles – Fresh particles and secondary aerosol formation☆

Pauli Simonen [a, *], Joni Kalliokoski [a], Panu Karjalainen [a], Topi Rönkkö [a], Hilkka Timonen [b], Sanna Saarikoski [b], Minna Aurela [b], Matthew Bloss [b], Georgios Triantafyllopoulos [c], Anastasios Kontses [c], Stavros Amanatidis [c, 1], Athanasios Dimaratos [c], Zissis Samaras [c], Jorma Keskinen [a], Miikka Dal Maso [a], Leonidas Ntziachristos [a, c]

[a] Aerosol Physics Laboratory, Physics Unit, Faculty of Engineering and Natural Sciences, Tampere University, Tampere, Finland
[b] Atmospheric Composition Research, Finnish Meteorological Institute, Helsinki, Finland
[c] Laboratory of Applied Thermodynamics, Aristotle University of Thessaloniki, Thessaloniki, Greece

ARTICLE INFO

Article history:
Received 4 June 2019
Received in revised form
19 August 2019
Accepted 3 September 2019
Available online 12 September 2019

Keywords:
RDE
Secondary organic aerosol
SOA
Particle number
PM

ABSTRACT

Emissions from passenger cars are one of major sources that deteriorate urban air quality. This study presents characterization of real-drive emissions from three Euro 6 emission level passenger cars (two gasoline and one diesel) in terms of fresh particles and secondary aerosol formation. The gasoline vehicles were also characterized by chassis dynamometer studies. In the real-drive study, the particle number emissions during regular driving were 1.1–12.7 times greater than observed in the laboratory tests (4.8 times greater on average), which may be caused by more effective nucleation process when diluted by real polluted and humid ambient air. However, the emission factors measured in laboratory were still much higher than the regulatory value of 6×10^{11} particles km^{-1}. The higher emission factors measured here result probably from the fact that the regulatory limit considers only non-volatile particles larger than 23 nm, whereas here, all particles (also volatile) larger than 3 nm were measured. Secondary aerosol formation potential was the highest after a vehicle cold start when most of the secondary mass was organics. After the cold start, the relative contributions of ammonium, sulfate and nitrate increased. Using a novel approach to study secondary aerosol formation under real-drive conditions with the chase method resulted mostly in emission factors below detection limit, which was not in disagreement with the laboratory findings.

1. Introduction

Traffic is an important source of both gaseous and particle pollutants (Hasheminassab et al., 2014; Pant and Harrison, 2013; Pérez et al., 2010; Rakowska et al., 2014). While the emissions of some of these pollutants are effectively regulated, the formation potential of secondary aerosol or emissions of small (<23 nm) and volatile particles are not directly controlled. European Regulations on vehicle exhaust particle emissions address the number of non-volatile particles with the size of a minimum 50% cutpoint at 23 nm (Commission Regulation (EU) 2017/1151). For light-duty vehicles, the particle number (PN) limit is set to 6×10^{11} particles km^{-1} and this is applicable to diesel vehicles and gasoline vehicles equipped with direct injection engines. This limit is now well

☆ This Paper has been recommended for acceptance by Dr. Admir Créso Targino.

* Corresponding author.
E-mail addresses: pauli.simonen@tuni.fi (P. Simonen), joni.kalliokoski@tuni.fi (J. Kalliokoski), panu.karjalainen@tuni.fi (P. Karjalainen), topi.ronkko@tuni.fi (T. Rönkkö), hilkka.timonen@fmi.fi (H. Timonen), sanna.saarikoski@fmi.fi (S. Saarikoski), minna.aurela@fmi.fi (M. Aurela), matthew.bloss@fmi.fi (M. Bloss), triantag@auth.gr (G. Triantafyllopoulos), akontses@auth.gr (A. Kontses), samana@caltech.edu (S. Amanatidis), adimaratos@auth.gr (A. Dimaratos), zisis@auth.gr (Z. Samaras), jorma.keskinen@tuni.fi (J. Keskinen), miikka.dalmaso@tuni.fi (M. Dal Maso), leon@auth.gr (L. Ntziachristos).
[1] Present address: Division of Chemistry and Chemical Engineering, California Institute of Technology, Pasadena, California, USA.

https://doi.org/10.1016/j.envpol.2019.113175

established and a thorough methodology exists on how to measure and quantify non-volatile particle emissions. However, it is not clear why we should only limit the emissions of this specific fraction of all exhaust particles. The vehicle exhaust plume in the atmosphere contains particle fractions of different volatility, including volatile, semi-volatile and non-volatile ones (Biswas et al., 2007; Momenimovahed et al., 2015; Wang et al., 2017), which have been formed either in the engine (Malmborg et al., 2017), during the dilution process (Rönkkö et al., 2006), or in the atmosphere by oxidation (Gentner et al., 2017). Second, it is long known that vehicular exhaust contains particles extending much below 23 nm (Kittelson, 1998). Third, the limit value of 6×10^{11} particles km^{-1} seems arbitrarily set, as it is not directly associated with any atmospheric, air quality or health specific targets (Giechaskiel et al., 2012). Thus, the current regulation, limited to only one fraction of particles, does not reflect the actual real-world exposure to aerosol emissions from traffic.

What seems to be a questionable regulation in its scientific underpinning, has actually been very effective in introducing advanced particle emission controls on actual vehicles. It has been effectively mandatory since 2009 that all new on-road diesel light-duty vehicles (and off-road engines since 2019) need to be equipped with diesel particle filters (DPFs). Moreover, the EU will be the first region in the world where the large majority of gasoline vehicles sold – those equipped with direct injection engines – will be equipped with gasoline particle filters (GPFs) to comply with PN limits.

The introduction of advanced emission control systems guarantees that the certified vehicles comply with exhaust PN limits. But the use of advanced emission control per se says little about the actual environmental performance of vehicles, as bitter experience from the diesel NOx scandal has recently revealed (Jonson et al., 2017). In assessing the actual impact, at least in terms of particle emissions, one will need to study both primary emissions but also the propensity of vehicle exhaust to form delayed primary particulate matter (PM) upon dilution (Rönkkö et al., 2017) and secondary PM after oxidation in the atmosphere (e.g. Chirico et al., 2010).

Real-world environmental impacts can be assessed by studying vehicles under actual operation and intervening as little as possible with the actual processes that take place between particle emission and atmospheric transformation. Chase experiments (e.g., Giechaskiel et al., 2005; Rönkkö et al., 2006) allow the vehicle to be studied under actual operation while its plume is diluted and dispersed in the atmosphere. However, this provides little time (~second) between emission and sampling for any oxidation reactions to occur. The use of an oxidation flow reactor (OFR; Simonen et al., 2017) in sampling plumes while chasing actual vehicles on the road can be a very powerful tool to study the exhaust's potential to form secondary PM under actual driving conditions. OFRs are needed to determine the organic proportion of the potential secondary aerosol (SOA; secondary organic aerosol) because it is difficult to estimate the SOA formation potential by measuring the gaseous organic precursor emissions (Gentner et al., 2017). For engine exhaust studies, OFRs have mainly been used under laboratory conditions (Friedman et al., 2017; Ihalainen et al., 2019; Jathar et al., 2017; Karjalainen et al., 2016; Link et al., 2017; Pieber et al., 2018; Timonen et al., 2017; Zhao et al., 2018), and to a smaller extent in roadside environments to study pass-by plumes from individual city buses running on different fuels (Watne et al., 2018) or emissions from a vehicle fleet (Liu et al., 2019; Ortega et al., 2016; Saha et al., 2018; Tkacik et al., 2014).

In this study, we present emission factors (EFs) of primary and secondary particle emissions from latest technology light-duty vehicles fueled by diesel and gasoline. The measurements were performed for all the vehicles on a racing track by chasing the vehicles with a mobile laboratory, and for the gasoline vehicles also in the laboratory on a chassis dynamometer. Overall, the study objective is to assess particle emissions under realistic operation environments in comparison to regulated driving cycles while, at the same time, allowing a comprehensive evaluation of all particulate matter emission dimensions relevant to urban air quality.

2. Materials and methods

Three Euro 6 light-duty vehicles were tested: a gasoline vehicle equipped with port fuel injection (PFI), a gasoline vehicle equipped with direct injection (GDI), and a diesel vehicle. The gasoline vehicles were equipped with three-way catalysts (TWC) and the diesel vehicle with a diesel oxidation catalyst (DOC), a diesel particulate filter (DPF) and a selective catalytic reduction device (SCR). The emissions of all three vehicles were measured in real-drive conditions by chasing, and the emissions of the two gasoline vehicles were additionally characterized by chassis dynamometer testing. The vehicle specifications are shown in detail in Table S1. Standard market fuel was used in all experiments, but the fuel used in the laboratory experiments was not necessarily from the same batch as the fuel used under real-drive tests.

2.1. Laboratory experiments

Chassis dynamometer testing was conducted in an emissions laboratory. The sampling setup for the laboratory measurements is shown in Fig. S1 and is described in detail in the Supporting Information (SI). Shortly, the engine exhaust was sampled from the tailpipe with a setup that has been shown to produce particle size distributions resembling those after a few seconds following atmospheric dilution (Keskinen and Rönkkö, 2010; Rönkkö et al., 2006), where the aerosol contains both nonvolatile primary particles and particle matter formed by condensation and nucleation. Regulated gas species (NO_x, CO, THC) were determined following vehicle certification regulations, utilizing a constant volume sampling (CVS) system.

Secondary aerosol formation potential was determined by a Tampere Secondary Aerosol Reactor (TSAR), by comparing the particulate mass downstream of the reactor to that of the untreated aerosol, measured in parallel. TSAR is an oxidation flow reactor (OFR) designed for measuring secondary aerosol formation of rapidly changing emission sources, such as vehicles during transient operation (Simonen et al., 2017). In this, the diluted exhaust is mixed with ozone and humidified air, and is then exposed to 254 nm UV radiation, where ozone photolysis produces OH radicals in the presence of H_2O. The oxidation reactions between precursor gases present in the exhaust and OH or O_3 lead to the formation of secondary aerosol.

Aerosol mass was measured with electrical low pressure impactors (Keskinen et al., 1992) (ELPI; Dekati Ltd.) with improved nanoparticle resolution (Yli-Ojanperä et al., 2010) by integrating the size distribution determined in impactor stages 1–7, corresponding to particles sized up to ~380 nm in aerodynamic diameter. One ELPI sampled the untreated aerosol, herein referred to as 'fresh' aerosol, and a second one was used downstream of TSAR to measure the 'aged' aerosol. The aged aerosol thus includes both fresh aerosol and secondary aerosol. Aerosol instrumentation was placed downstream of three-way valves, to selectively measure either aged or fresh sample. This included an engine exhaust particle sizer (Johnson et al., 2004) (EEPS; TSI Inc.), an ultrafine condensation particle counter (CPC; CPC 3776, TSI Inc.), a scanning mobility particle sizer (SMPS), and a soot-particle aerosol mass spectrometer (Onasch et al., 2012) (SP-AMS; Aerodyne Research Inc.). Moreover, a CO_2 analyzer (Sick Maihak, Sidor) was used to

determine the dilution ratio (DR) at different stages of dilution during steady state driving at 80 km h^{-1}, by comparing upstream and downstream CO_2 concentrations.

A SP-AMS (described in detail in the SI) was used to measure the aerosol mass content in total organic aerosol (OA), ions (sulfate, nitrate, ammonium) and refractive black carbon (rBC). Due to the limited time resolution and the dropping detection efficiency of the SP-AMS for small particles, this was only used here to determine particle composition, while mass concentration was determined from ELPI size distributions. For example, the organic mass concentration (M_{org}) is defined by

$$M_{org} = \frac{OA_{AMS}}{TOT_{AMS}} \times M_{ELPI}, \quad (1)$$

where OA_{AMS} is the organic aerosol mass and TOT_{AMS} is the total mass, respectively, measured by the SP-AMS, and M_{ELPI} is the ELPI-determined mass concentration. This approach implicitly assumes that the composition of small particles not detected by the SP-AMS is the same as the particles actually being measured. This assumption is a source of uncertainty for the composition-specific emission factors. However, the effect of the particles below SP-AMS detection limit on the total mass is generally small, as demonstrated in the average mass size distributions in Figs. S4b–c.

While ELPI is advantageous because of its high time resolution, it does not measure the mass directly and thus introduces uncertainty in the particle mass EFs. This uncertainty is evaluated in the SI (Fig. S9) by comparing the mass determined from ELPI size distributions to gravimetrically determined mass EFs, and by intercomparison between ELPI and EEPS. Shortly, there is a good agreement between ELPI and EEPS for the fresh aerosol mass, but the gravimetric mass is always higher. For the aged aerosol, the mass determined from ELPI is approximately three times higher than that from EEPS. This may partly depend on the assumption of unit density, but it is also possible that the aged mass determined from ELPI is slightly overestimated.

In the laboratory experiments, the driving cycles were the cold-start New European Driving Cycle (NEDC), the warm-start NEDC, and the warm-start Worldwide Harmonized Light Vehicles Test Cycle (WLTC). In addition, steady state driving at 80 km h^{-1} was measured for each vehicle. The laboratory schedule is presented in Table S2. Only one cold-start NEDC and warm-start WLTC were measured for each vehicle, and the SP-AMS measured the aged sample during these cycles. Thus, the concentration of fresh OA is unknown in these cases and the amount of potential SOA is approximated by assuming that all fresh aerosol is organic, which may underestimate the SOA formation potential. For the warm-start NEDC and 80 km h^{-1} steady cycles, the composition of fresh aerosol was measured (although during a separate driving cycle for the warm-start NEDC), so the SOA production factor (PF) is calculated by subtracting the fresh OA EF from the aged OA EF. The sampling setup was not functioning during the cold-start NEDC for the PFI, and thus no particle emission data is available for this driving cycle.

EFs were determined for the total driving cycles but also for specific sections in the cycles, which are hereafter called 'slow acceleration' and 'fast acceleration'. The EFs for slow accelerations are calculated from four identical acceleration phases of warm-start NEDCs, where the vehicle accelerates from 0 to 50 km h^{-1}. The fast acceleration EF is calculated from the warm-start WLTC at 958 s after start, where the vehicle accelerates from 25 to 50 km h^{-1}.

2.2. Real-driving experiments

The real-driving emissions were determined by chase measurements. The chase experiments were conducted at the Sérres racing track, Greece (41°04′20.9″N 23°31′01.4″E; track length 3.2 km). The track is located 3 km southwest of Sérres city center and is surrounded by fields. The measurements lasted for three days, and the schedule with associated ambient conditions is presented in Tables S2–3. All vehicles were equipped with a Portable Emissions Measurement System (PEMS; AVL M.O.V.E Gas PEMS iS) to measure second by second concentrations of CO, CO_2, NO and NO_2 in the tailpipe. In addition, the on-board diagnostics (OBD) data and vehicle coordinates from a GPS device were logged.

The vehicles were chased by the Tampere University Mobile Laboratory, which is a large van equipped with stainless steel sampling lines and instruments to measure exhaust emissions (Rönkkö et al., 2017). The sample was drawn from the lower-mid sampling line at the front of the vehicle, which is located approximately 50 cm above ground. A weather station (Weather Station 200WX; Airmar Technology Corporation) on the roof of the van recorded the ambient temperature, humidity and the coordinates from GPS. The sampling setup is shown in Fig. S10. The sample was drawn directly to a CO_2 analyzer, ELPI, CPC and TSAR. Similar to the lab measurements, the first ELPI was used to determine fresh aerosol mass and a second ELPI downstream of TSAR determined aged aerosol concentrations. A low dilution of 1.9:1 preceding the second ELPI was necessary to keep the total flow rate through the upstream TSAR at 5 lpm. The SP-AMS was installed in the mobile laboratory, but it was not possible to distinguish the composition of exhaust aerosol from the dominating background mass.

All the vehicles drove similar driving patterns at the track: regular driving with varying speed and stops, steady state driving at 80 km h^{-1}, slow accelerations from 0 to 50 km h^{-1} (identical to the accelerations in the NEDC), and fast accelerations from 20 km h^{-1} to 50 km h^{-1} (resembling a fast acceleration in the WLTC). The steady state driving at 80 km h^{-1} performed on-road is not directly comparable to the laboratory steady driving. In the laboratory, the vehicle was allowed to stabilize after reaching the speed of 80 km h^{-1}, whereas on the track, the measurement started directly after the acceleration, so that some of the particles measured may actually have originated from the acceleration rather than from the steady speed driving, which lasted for approximately 10 s. In addition, the chassis dynamometer NEDC slow acceleration was not representative of the real-drive slow acceleration despite the similar speed profiles, because the type-approval dynamometer load setting in the NEDC was not the same as the actual road load (Mock et al., 2012). The engine was warmed up by driving at least 5 min before the actual measurements.

2.3. Data analysis

Emission factors (EF) of any compound were determined by eq. (2):

$$EF = \frac{\int \left([C](t) - \left[C_{bg}\right](t) \right) \times DR(t) \times Q_{exh}(t) dt}{N}, \quad (2)$$

where $[C]$ is the time-dependent concentration, $[C_{bg}]$ is the background concentration, DR is the total dilution ratio, Q_{exh} is the volumetric exhaust flow and N is the quantity to which emissions are normalized (e.g., fuel consumed or distance travelled). In laboratory experiments, the volumetric exhaust flow was calculated from the flow rate and the DR of the CVS. In chase experiments, the exhaust flow was calculated from the engine intake air pressure or intake airflow data combined with the PEMS gas concentration data (SI). The secondary mass PFs were calculated by subtracting the fresh aerosol mass EFs from the aged mass EFs.

In the laboratory measurements, *DR* was constant and $[C_{bg}]$ was zero except for the aged mass. The aged mass background was determined by oxidizing pure humidified dilution air with TSAR. In the chase measurements, *DR* depends on the chase distance and the plume behavior, and was calculated by eq. (3):

$$DR(t) = \frac{[CO_{2,raw}](t) - [CO_{2,bg}](t)}{[CO_{2,dil}](t) - [CO_{2,bg}](t)}, \quad (3)$$

where $[CO_{2,raw}]$ is the raw exhaust CO_2 concentration measured by PEMS, $[CO_{2,bg}]$ is the background CO_2 concentration, and $[CO_{2,dil}]$ is the CO_2 concentration measured by the mobile laboratory. When defining the EF for the aged aerosol (downstream of TSAR), $[CO_{2,raw}]$ and Q_{exh} are convolved with the residence time distribution of TSAR to take the TSAR delay into account (SI). When calculating the real-drive EFs, we neglect the data where DR was negative or higher than 6000:1.

To determine the background concentrations in real-drive measurements, we assumed that due to the required distance between the mobile laboratory and the vehicle chased, the in-van instruments occasionally unintentionally sampled background air instead of the exhaust plume even when chasing the vehicle. Thus, for a CO_2 value measured at time t ($[CO_{2,dil}(t)]$), we define the background concentration ($[CO_{2,bg}(t)]$) as the third CO_2 concentrations percentile between t-2 min and t+2 min. The background number and mass concentrations measured by CPC and ELPIs were defined similarly, but the 15th percentile was used because of the higher deviation in the particle measurements. A comparison between the calculated background levels and the actual background concentrations measured while not chasing a vehicle is shown in Fig. S11.

While this approach is suitable to estimate the regional background, it cannot distinguish short peaks of background pollutants from the vehicle exhaust. As a result, the potential noise in background concentration causes a bias in the EF calculated by eq. (2). To estimate the effect of varying background emissions on the calculated EFs, we performed reference measurements by driving around the track without chasing any vehicle. Based on these measurements, we determined the background noise level for the emission factor (EF_{bg}) for each chase measurement by means of eq. (4):

$$EF_{bg} = \frac{\int [C_{ref}] \times DR(t) \times Q_{exh}(t)dt}{N}, \quad (4)$$

where $[C_{ref}]$ is the average background-corrected concentration of the pollutant during the closest reference measurement, whereas *DR*, Q_{exh} and *N* are the values from the actual chase measurement. Effectively, EF_{bg} defines the EF that would be calculated for a vehicle with no pollutant emissions, and this EF will be nonzero due to the noise in the background concentrations. A similar approach to define EFs below threshold has been used by Wang et al. (2015).

3. Results and discussion

Particle emissions and secondary aerosol formation potential are discussed in the following sections. The EFs are normalized to the distance travelled, with emissions normalized to fuel consumed available in the SI. The regulated emissions measured both in laboratory and under real-drive conditions are presented in Table S4.

3.1. Emission factors of particle number

Fig. 1a shows the fresh background-corrected average particle number concentrations measured by a CPC during fast accelerations in chase experiments. The corresponding vehicle speeds and background-corrected CO_2 levels are shown in Fig. 1b. The highest particle number concentrations were measured when chasing the PFI, while only a small peak in concentration is observed in the wake of the diesel vehicle. However, due to different dilution ratios, it is necessary to compare the EFs instead of the absolute particle concentrations.

Emission factors for fresh particle number for the laboratory measurements are shown in Fig. 2a–b. Values in Fig. 2a correspond to particles above 3 nm measured by a CPC, whereas Fig. 2b shows values corresponding to particles larger than 7 nm, as measured by an ELPI. The error bars for laboratory measurements in Fig. 2 show the standard deviation of two or more repetitions, and EFs without error bars are calculated from a single measurement. Fresh particle emissions of both gasoline vehicles exceeded the limit defined in the Euro 6 regulation. This is only to put levels into perspective, as fresh particles include volatile and semi-volatile ones and range down to 3 nm, while the limit only addresses non-volatile particles larger than 23 nm from diesel and GDI vehicles. The results obtained in the lab indicate that PFI vehicles that are not controlled by regulations emit significant numbers of fresh particles.

The average real-drive EFs for particles larger than 3 nm and 7 nm are shown in Fig. 2c–d along with the average background noise levels. The error bars for the real-drive EFs indicate the minimum and maximum values of the calculated EFs. For the cases where EFs are close to or below the background noise, the actual EF can be anything between zero and the measured EF.

The diesel vehicle EFs were below or very close to the background noise level, indicating low particle emissions. This shows that the DPF was effective at controlling total fresh particle

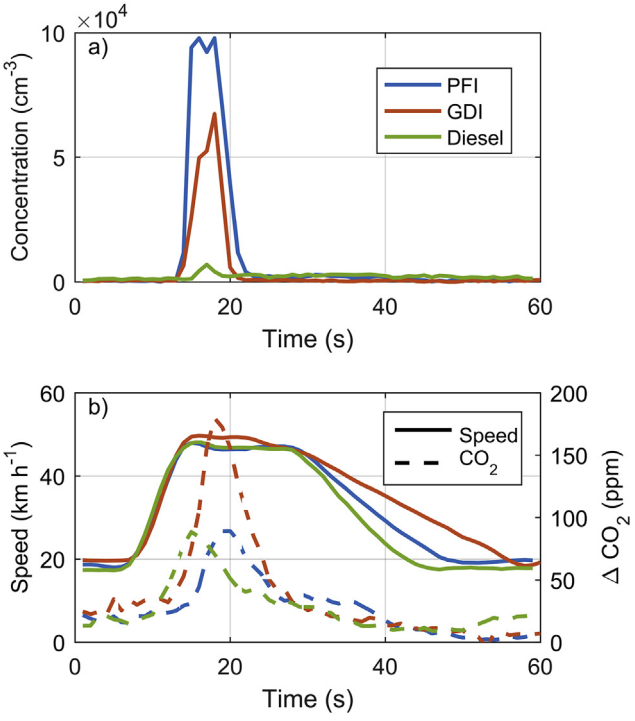

Fig. 1. The average background-corrected particle concentrations in the exhaust plume measured by CPC during real-drive fast accelerations (a), and the corresponding average speeds and background-corrected CO_2 concentrations (b).

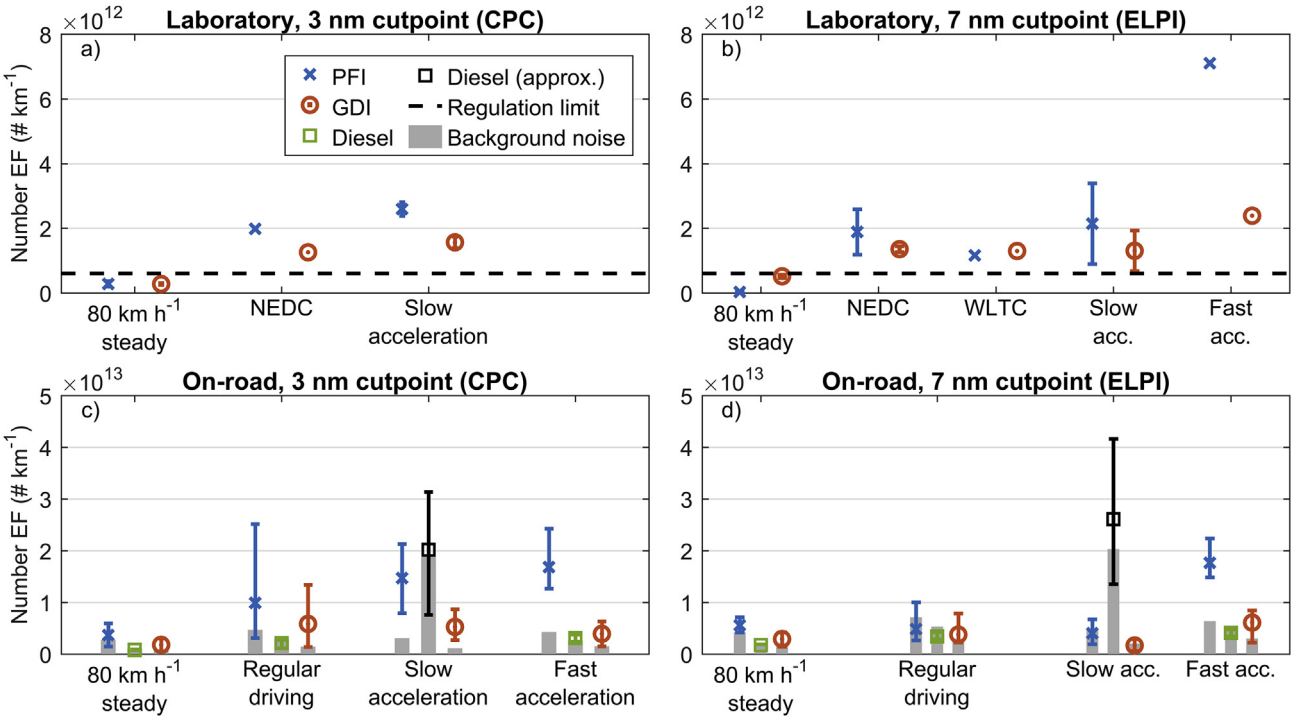

Fig. 2. Fresh particle number emission factors. Average laboratory EFs of particles larger than 3 nm (a), laboratory EFs of particles larger than 7 nm (b), real-drive EFs of particles larger than 3 nm (c) and real-drive EFs of particles larger than 7 nm (d). The CPC data is not available for the WLTC (including the fast acceleration) measurement in the laboratory. Note the different scales for laboratory and real-drive measurements.

emissions, even during real-world driving. Only during slow accelerations did diesel emissions occasionally appear higher than the average background. These cases had higher uncertainties, since the *DR* and Q_{exh} were approximated based on the fast acceleration data, as the PEMS was not functioning during the slow acceleration cases driven with the diesel vehicle. The *DR* was approximated by assuming an inverse correlation between *DR* and the measured CO_2, and acquiring the fitting parameter from the fast acceleration cases. Similarly, we assumed that Q_{exh} depends on vehicle speed and acceleration, and fitted a polynomial function to these parameters for the fast acceleration cases and used the same fits for the slow accelerations. The high variation in the slow acceleration EFs and the difference in the absolute level of the EFs (compared to regular driving and fast acceleration cases) suggest that the high EFs may also be an artefact from a background source or that the vehicle occasionally emits high amounts of particles during this acceleration due to factors such as DPF regeneration or a storage-release phenomena of semivolatile particle precursors in the aftertreatment system (Karjalainen et al., 2014a).

On the contrary, a clear signal for particles larger than 3 nm was produced by the petrol vehicles, with the PFI being higher than the GDI, similar to the laboratory results. In addition, there was more absolute variation in the EFs for the PFI than the other vehicles, which may indicate unstable operation of the PFI under real-driving conditions. The difference between the PFI and GDI was largest during accelerations, where the PFI emitted 3–4 times more particles than the GDI. The PFI particle emissions were more sensitive to the driving condition than the GDI, since the EF of fast acceleration for the PFI was 4.6 times higher than that of steady state driving at 80 km h^{-1}, whereas for the GDI, this ratio was 2.2.

Both gasoline vehicles emitted more particles under real-drive conditions than in laboratory driving based on the EFs determined by CPC. However, the difference between the real-drive and laboratory EFs was much higher for the PFI than the GDI. For example, in slow acceleration the PFI real-driving EF was 5.7 times the laboratory EF, whereas the GDI real-driving EF was 3.4 times the laboratory EF.

More small particles (approximately in range 3–7 nm) were emitted or nucleated under real-drive conditions than in the laboratory based on the EFs determined from the CPC with 3 nm cutpoint and ELPI with 7 nm cutpoint. In the laboratory experiments, the EFs calculated based on the number concentration measured by ELPI and CPC were almost equal, whereas in real-drive measurements the CPC-originated EFs were significantly higher during regular driving and slow acceleration while the ELPI-originated EFs were often close to or below the detection limit. There are several possible reasons for the higher amount of the small particles under real-drive conditions. First, the vehicle operation during the real-drive test may differ from the laboratory operation because of factors such as different engine loads. For example, the average real-driving CO_2 EFs for regular driving were 1.4–1.5 times higher than the laboratory cycle EFs (Table S4). Second, the driving history can be different, leading to a difference in storage-release phenomena of particle precursors in the catalyst, which affect the nucleation mode particle emissions (Karjalainen et al., 2014b, 2014a). Third, nucleation mode particle formation is sensitive to the relative humidity and temperature of the dilution air (Rönkkö et al., 2006). Even though the laboratory sampling setup simulates the atmospheric delayed primary particle formation, the used 30 °C dry dilution air may not be able to simulate the actual particle formation in the real-drive conditions in this study, where the average ambient temperatures were 11.8–17.7 °C and relative humidity was higher than 50%. It has been shown earlier that the EFs of volatile particles are higher at lower temperatures (Wang et al., 2017), and the relative humidity affects at least the nucleation dynamics of sulfuric acid and water (Brus et al., 2010).

Previous studies have shown that the particle EFs for GDI vehicles usually exceed those for the PFI vehicles (Chen et al., 2017;

Mamakos et al., 2012; Zhu et al., 2016). The results obtained in this study both in laboratory and under real-drive conditions seem to disagree with the previous studies, since we found higher particle number EFs for the PFI vehicle. However, this is not necessarily a disagreement, since the measurement technique in this study differs from the aforementioned studies. We measured all particles larger than 3 nm, whereas the previous studies report the EFs for solid particles only. Thus, it is possible that the higher EFs for the PFI observed here result from higher emissions of volatile particles.

The hypothesis is supported by the particle number size distributions in Fig. S4a. The accumulation mode, which often contains non-volatile soot particles, is higher for the GDI, whereas the nucleation mode is higher for the PFI. A similar phenomenon was observed by Saliba et al. (2017). We note that we cannot make strong conclusions regarding the two engine technologies because only two vehicles were tested, and we cannot distinguish the solid and volatile fractions based on our measurements.

3.2. Emission factors of particle mass

Because of the low signal-to-noise ratio, the actual real-driving EFs for the fresh and aged aerosol mass could not be determined in most cases. Thus, we only shortly discuss the results here, and show the emission factors in Fig. S12.

In the laboratory, the EFs for both gasoline vehicles were less than 0.2 mg km^{-1}, except for the fast acceleration case, where the PFI emitted 0.85 mg km^{-1} and the GDI 0.25 mg km^{-1}. In real-drive conditions, the average EFs were below the average background noise levels except for the slow acceleration of the diesel vehicle. This is similar to what was observed for the particle number emissions of the diesel vehicle.

The particulate mass of the aged exhaust in laboratory experiments was always higher than the fresh aerosol mass, and is discussed in Sect 3.3. In real-drive measurements, it was challenging to determine the secondary aerosol formation by the chase method due to the high background noise in the aged mass, similar to the fresh aerosol mass measurements. The only case where the average aged aerosol EF was higher than the background noise was the fast acceleration with the PFI, which also produced the highest EF in the laboratory measurements. However, the real-drive EF in this case was lower than the laboratory EF, and also in the other cases the real-drive EFs of the aged mass were close to the laboratory EFs despite the background influence (Fig. S12). Thus, even though the background noise prevented the determination of exact PFs for the secondary mass, we can deduce that the secondary aerosol formation potential under real-drive conditions was not significantly higher than in laboratory measurements.

3.3. Aged exhaust aerosol in laboratory

The time series of aged organic aerosol mass (average 7–13 days equivalent atmospheric aging; see Fig. 4 and Fig. S2) and fresh aerosol mass measured for the laboratory driving cycles and one real-drive cold start are shown in Fig. 3. To make the fresh aerosol mass and aged mass comparable, the fresh aerosol mass data in the figure is convolved with the TSAR residence time distribution. An average mass particle size distribution of the aged aerosol during an acceleration is shown in Fig. S4c, and the time-resolved particle number size distributions of the aged aerosol during the NEDCs and the WLTCs are shown in Figs. S6 and S8, respectively.

We do not have a direct measurement of SOA formation from the exhaust because the fresh OA was not measured simultaneously with the aged OA. However, when the aged OA is higher than the total fresh aerosol mass, there is obviously SOA formation in TSAR. The most apparent transient SOA formation phenomenon is observed during the GDI cold-start driving cycle (Fig. 3a). The SOA formation begins immediately after the engine start and exceeds the SOA observed during the hot-start cycle by approximately a factor of 25 at maximum. This is reflected in the SOA production factor so that the GDI cold-start NEDC produces 5 times more SOA than the hot NEDC (Fig. 4). Approximately 200 s after the cold start, the aged OA levels off, and its profile for the rest of the cycle is close to that of the hot-start cycle. A similar secondary aerosol formation event was observed for the PFI cold-start at track conditions, measured with the chase measurement set-up (Fig. 3d). This is the only case where a clear signal above the detection limit could be obtained for the aged mass under real-drive conditions, as discussed in the previous section. Thus, in this section, we analyze only the aged mass determined in the laboratory studies.

The high SOA formation in the beginning of the cold-start cycles has been reported in several earlier publications (Karjalainen et al., 2016; Pieber et al., 2018; Timonen et al., 2017), and is most probably related to the catalyst temperature. Specifically, the catalyst temperature during cold start is too low to oxidize the emitted hydrocarbons and thus they are available for oxidation in the OFR. By using the TSAR designed for high time resolution, it allows us to analyze driving condition dependent SOA formation, in contrast to other publications using the potential aerosol mass (PAM) reactor (Kang et al., 2007; Lambe et al., 2011) (see SI).

The SOA formation from the PFI exhaust in the TSAR seems to depend strongly on driving condition, as it was the case for both number and mass EFs. For the PFI hot NEDC (Fig. 3b), there was a peak in SOA formation both in the beginning of the cycle during the first acceleration from 0 to 30 km h^{-1} and at the end of the cycle during high speed driving and acceleration from 100 to 120 km h^{-1}. For the PFI hot WLTC (Fig. 3e), there were several peaks in the aged OA, the highest ones again in the beginning of the cycle and for the acceleration at the end of the cycle. On the other hand, the SOA formation decreased when driving at a relatively constant speed of 90 km h^{-1} starting from 1200 s after the start of the WLTC.

The SOA formation from the GDI exhaust showed much less transient behavior than the PFI. For the NEDC (Fig. 3c), the aged OA was relatively constant throughout the cycle with a slight increase for the high-speed part of the cycle. The absolute levels of aged OA were almost equal in the WLTC and in the NEDC, except for a few peaks during high-speed driving at the end of the WLTC.

The differences between the two gasoline vehicles regarding the SOA formation in the TSAR are evident in Fig. 4, where the total SOA production factors are presented. The steady driving at 80 km h^{-1} and hot WLTC with PFI had the lowest and highest PFs of SOA at hot engine operation, respectively, with 3.5 times difference between the two. In contrast, the production of SOA with GDI was almost independent of driving conditions, since the steady state driving at 80 km h^{-1} produced almost equal amount of SOA as the other warm-start driving cycles. The differences in SOA production demonstrate vehicle-to-vehicle variation and cannot be addressed to the different gasoline injection technologies since only two vehicles were tested. A larger set of vehicles was tested by Zhao et al. (2018) in an engine laboratory. Using a PAM reactor, they found no difference between GDI and PFI vehicles in total SOA production integrated over the phases of a driving cycle. However, it is not possible to analyze the dependence of SOA formation on specific driving conditions by using a PAM reactor because of its long residence time. Thus, the two engine technologies may behave differently in terms of SOA production under transient driving conditions even when the integrated SOA production over a certain test cycle is equal.

Most previous studies on gasoline vehicle SOA formation potential report SOA PFs only for cold-start driving cycles (Karjalainen et al., 2016; Pieber et al., 2018; Timonen et al., 2017; Zhao et al.,

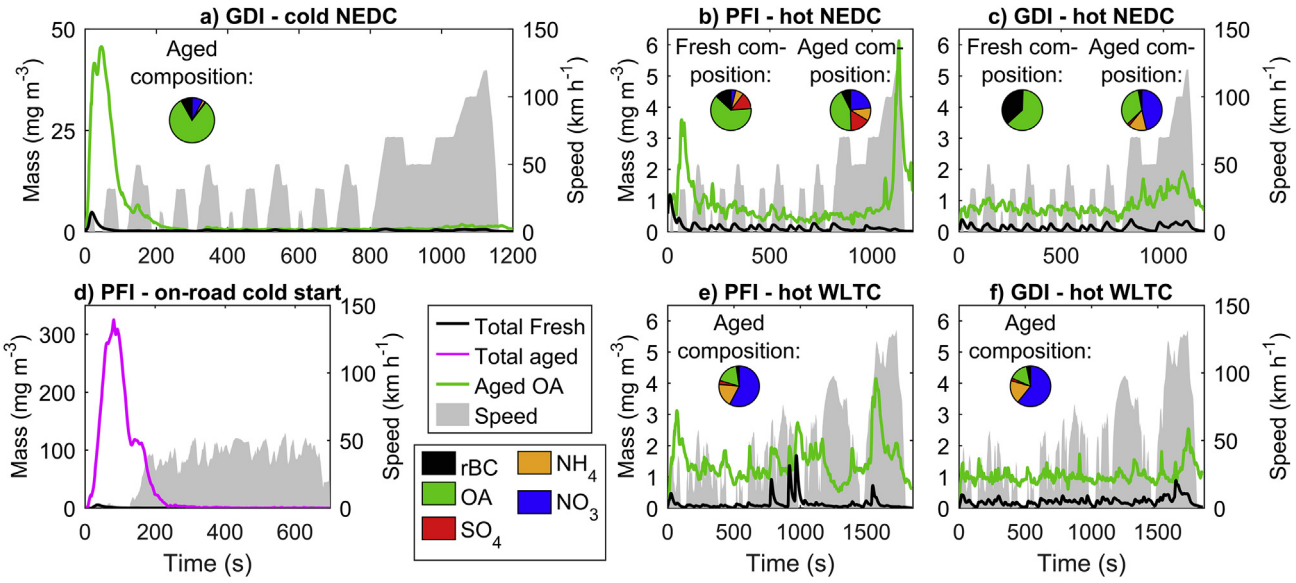

Fig. 3. Time series of aged organic aerosol and total fresh aerosol mass concentrations, calculated to raw exhaust. The average aerosol compositions measured by SP-AMS are shown in pie charts. For the time series of other chemical compounds, see Fig. S17. All panels show mass concentrations measured in the engine laboratory, except (d), which shows the PFI cold start in on-road conditions.

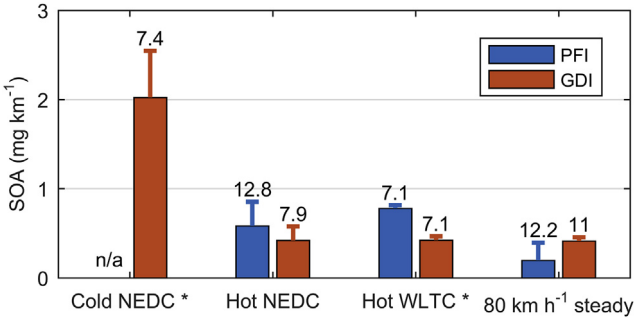

Fig. 4. SOA PFs determined from the laboratory experiments. The numbers above the bars indicate the average OH exposure during the cycles (as equivalent atmospheric days). Error bars show the uncertainty related to potential losses of low volatility organic compounds in TSAR (SI). The cold NEDC of the PFI is excluded because of dilution system malfunction in the beginning of the cycle. *assuming all fresh aerosol is organic.

2018). The GDI cold-start NEDC SOA formation potential observed here is on the same order of magnitude as PFs of previous publications. Also, the warm-start SOA PFs agree with previously reported SOA PFs of warm-start cycles (Gordon et al., 2014a) (0–20 mg kg_{fuel}^{-1}) and warmed-up phases of cold-start cycles (Karjalainen et al., 2016; Pieber et al., 2018) (0.5–1.5 mg km^{-1} and 5–15 mg kg_{fuel}^{-1}).

To give a perspective on vehicle SOA formation potential, we compare the warm-start cycle SOA PFs measured in laboratory to SOA PFs from large vehicle fleets determined by roadside and tunnel measurements. The SOA PFs reported for vehicle fleets are 200–400 mg kg_{fuel}^{-1} (at 1–8 days eq. photo-oxidation) (Liu et al., 2019; Tkacik et al., 2014) or 40–190 $\mu g\, m^{-3}\, ppm^{-1}$ (at 2–9 days eq. photo-oxidation; normalized to CO concentration) (Saha et al., 2018). These values are much higher than the 8–21 mg kg_{fuel}^{-1} or 2–15 $\mu g\, m^{-3}\, ppm^{-1}$ (Figs. S15–16) measured here for the hot-engine operation, which indicates that the SOA formation potential from Euro 6 gasoline vehicles is significantly lower than that of the average fleet in these studies. Even though the Euro 6 values here were measured in the laboratory, the real-drive SOA formation potential of these vehicles is not expected to be significantly higher, because the real-drive measurements were below the detection limit as discussed in Section 3.2 and close to the values measured in the laboratory (Fig. S12). However, a significant difference between this study and the results from larger vehicle fleets is that the latter are measurements of a complex mixture of vehicle exhaust and urban air, whereas we sampled the exhaust of only one vehicle at time.

Even though the SOA formation from Euro 6 gasoline vehicles in this study is lower than that of the vehicle fleets spanning a wide range of model years, it is not guaranteed that the modernization of the vehicle fleet results in lower ambient SOA formation. The oxidation pathways of SOA precursors depend on the ambient NO_X concentrations, and decreasing NO_X concentrations may lead to increased SOA formation, despite the low-emitting vehicles (Zhao et al., 2017).

The diesel vehicle emissions were not measured in laboratory conditions. However, we note that previous research showed negligible SOA formation from diesel vehicles equipped with DPFs (Gordon et al., 2014b; Platt et al., 2017). We also measured the aged aerosol mass of another Euro 6 diesel vehicle in the emission laboratory (SI), and found that the aged OA mass was usually below the detection limit. Occasionally, we observed peaks of mass in the aged exhaust of the diesel vehicle at the end of the cycles, but this consisted mainly of ammonium nitrate and the highest peak was related to a regeneration of the DPF (Fig. S3).

The average aerosol compositions presented in Fig. 3 show that the dominant part of aged mass for both gasoline vehicles is inorganic. Mostly the aged inorganic mass is ammonium nitrate, but also a significant contribution of sulfate is observed for the PFI during the NEDC. Some of the sulfur is in the gas phase prior to TSAR because the SO_4:rBC ratio is higher in the aged aerosol than in the fresh aerosol. The precursor for the secondary sulfate aerosol is presumably SO_2, which oxidizes in TSAR to form SO_3, which further produces sulfuric acid. Maricq et al. (2002) have shown that during the beginning of a driving cycle, the sulfur from the gasoline vehicle exhaust is stored in the three-way catalyst, from where it is released as SO_2 during fast accelerations at the end of the cycle. The behavior of sulfur in PFI exhaust in the NEDC here seems to be

consistent with the observations by Maricq et al. as the sulfate is formed in TSAR at the end of the cycle (Fig. S17).

The secondary ammonium nitrate is formed when the ammonia in the exhaust reacts with nitric acid. Nitric acid (HNO_3) in TSAR is formed when the NO in the exhaust reacts with O_3 to form NO_2, and NO_2 further reacts with OH to form HNO_3. Thus, whenever there is ammonia and NO or NO_2 present in the exhaust, there will be ammonium nitrate formation in TSAR. The ammonia in gasoline vehicle exhaust is formed in the three-way catalyst (Heeb et al., 2006) and both ammonia emissions (Suarez-Bertoa et al., 2014; Suarez-Bertoa and Astorga, 2016) and formation of secondary ammonium nitrate from gasoline vehicle exhaust are frequently observed (Link et al., 2017; Nordin et al., 2013; Pieber et al., 2018).

4. Conclusions

The number emissions of fresh particles larger than 7 nm for three Euro 6 vehicles measured in this study in real-drive use were generally below background noise. However, by extending the measured particle size range down to 3 nm, we observed that the real-drive particle emissions for the gasoline vehicles were significantly higher than the corresponding emissions measured in laboratory, whereas the diesel vehicle emissions also in this size range were below background noise levels. The results cannot be generalized to different engine or aftertreatment technologies, but the high vehicle-to-vehicle variation highlights the need for real-drive tests to gain knowledge on exposure-relevant particle emissions and implications on air quality. Clearly, the current regulated particle emissions, considering only solid particles larger than 23 nm, do not reflect the actual emissions for all of the three vehicles measured here, despite all of them belonging to the same Euro 6 class.

In addition, the real-drive secondary aerosol formation potential was below the detection limit, and thus we expect that the laboratory-derived SOA production factors are representative of real driving SOA formation potential. The SOA PFs determined in the laboratory for warmed-up Euro 6 gasoline vehicles are approximately a tenth of the SOA PFs measured for vehicle fleets, and even lower for DPF equipped diesel vehicles according to this study and two others (Gordon et al., 2014b; Platt et al., 2017). Thus, increasing the proportion of Euro 6 light-duty vehicles in the vehicle fleet will likely diminish the atmospheric traffic-related SOA formation. However, Zhao et al. (2017) showed that transformation to modern gasoline vehicles does not necessarily reduce the SOA concentrations if the ambient NO_x levels decrease simultaneously. In addition to SOA, a comparable amount of inorganic secondary aerosol was formed from gasoline vehicle exhaust, mainly consisting of ammonium nitrate. Regulation of ammonia emissions should be considered to mitigate the effect of gasoline vehicles on urban air quality (Link et al., 2017).

Due to relatively low emissions of the studied Euro 6 vehicles, it was usually difficult to distinguish the vehicle emissions from the background when chasing a single vehicle. Thus, sampling the exhaust directly from the tailpipe as in PEMS applications may be better suitable for real-drive emission measurements than the chase method. However, this would require a specific dilution system for the fresh PN and the aged aerosol measurement. It is not clear whether the differences in EFs for particle number between laboratory and chase measurement were a function of the atmospheric dilution process or different vehicle operation. If the higher EFs were caused by nucleation during the atmospheric dilution (as discussed by Keskinen and Rönkkö, 2010), a PEMS dilution system may not be able to replicate the atmospheric particle formation and would not report exposure-relevant EFs for particle number. In addition, fitting all the equipment needed for the fresh PN and aged aerosol measurement on-board of a light-duty vehicle would be challenging. Another option to determine EFs for low-emitting vehicles is to conduct the chase experiments in a cleaner environment.

Funding

This work was supported by the Health relevant and energy efficient regulation of exhaust particle emissions (HERE) project [decision number 40330/13], funded by Business Finland (Tekes), AGCO Power Oy, Dinex Finland Oy, Dekati Oy, Neste Oyj, Pegasor Oy and Wärtsilä Finland Oy.

Pauli Simonen and Joni Kalliokoski acknowledge Tampere University Graduate School.

Appendix A. Supplementary data

Supplementary data to this article can be found online at https://doi.org/10.1016/j.envpol.2019.113175.

References

Biswas, S., Ntziachristos, L., Moore, K.F., Sioutas, C., 2007. Particle volatility in the vicinity of a freeway with heavy-duty diesel traffic. Atmos. Environ. 41, 3479–3493. https://doi.org/10.1016/j.atmosenv.2006.11.059.

Brus, D., Hyvärinen, A.-P., Viisanen, Y., Kulmala, M., Lihavainen, H., 2010. Homogeneous nucleation of sulfuric acid and water mixture: experimental setup and first results. Atmos. Chem. Phys. 10, 2631–2641. https://doi.org/10.5194/acp-10-2631-2010.

Chen, L., Liang, Z., Zhang, X., Shuai, S., 2017. Characterizing particulate matter emissions from GDI and PFI vehicles under transient and cold start conditions. Fuel 189, 131–140. https://doi.org/10.1016/j.fuel.2016.10.055.

Chirico, R., Decarlo, P.F., Heringa, M.F., Tritscher, T., Richter, R., Prévôt, A.S.H., Dommen, J., Weingartner, E., Wehrle, G., Gysel, M., Laborde, M., Baltensperger, U., 2010. Impact of aftertreatment devices on primary emissions and secondary organic aerosol formation potential from in-use diesel vehicles: results from smog chamber experiments. Atmos. Chem. Phys. 10, 11545–11563. https://doi.org/10.5194/acp-10-11545-2010.

Commission Regulation EU, 2017. Commission Regulation (EU) 2017/1151 of 1 June 2017. Off. J. Eur. Union.

Friedman, B., Link, M.F., Fulgham, S.R., Brophy, P., Galang, A., Brune, W.H., Jathar, S.H., Farmer, D.K., 2017. Primary and secondary sources of gas-phase organic acids from diesel exhaust. Environ. Sci. Technol. 51, 10872–10880. https://doi.org/10.1021/acs.est.7b01169.

Gentner, D.R., Jathar, S.H., Gordon, T.D., Bahreini, R., Day, D.A., El Haddad, I., Hayes, P.L., Pieber, S.M., Platt, S.M., de Gouw, J., Goldstein, A.H., Harley, R.A., Jimenez, J.L., Prévôt, A.S.H., Robinson, A.L., 2017. Review of urban secondary organic aerosol formation from gasoline and diesel motor vehicle emissions. Environ. Sci. Technol. 51, 1074–1093. https://doi.org/10.1021/acs.est.6b04509.

Giechaskiel, B., Mamakos, A., Andersson, J., Dilara, P., Martini, G., Schindler, W., Bergmann, A., 2012. Measurement of automotive nonvolatile particle number emissions within the European legislative framework: a review. Aerosol Sci. Technol. 46, 719–749. https://doi.org/10.1080/02786826.2012.661103.

Giechaskiel, B., Ntziachristos, L., Samaras, Z., Scheer, V., Casati, R., Vogt, R., 2005. Formation potential of vehicle exhaust nucleation mode particles on-road and in the laboratory. Atmos. Environ. 39, 3191–3198. https://doi.org/10.1016/j.atmosenv.2005.02.019.

Gordon, T.D., Presto, A.A., May, A.A., Nguyen, N.T., Lipsky, E.M., Donahue, N.M., Gutierrez, A., Zhang, M., Maddox, C., Rieger, P., Chattopadhyay, S., Maldonado, H., Maricq, M.M., Robinson, A.L., 2014a. Secondary organic aerosol formation exceeds primary particulate matter emissions for light-duty gasoline vehicles. Atmos. Chem. Phys. 14, 4661–4678. https://doi.org/10.5194/acp-14-4661-2014.

Gordon, T.D., Presto, A.A., Nguyen, N.T., Robertson, W.H., Na, K., Sahay, K.N., Zhang, M., Maddox, C., Rieger, P., Chattopadhyay, S., Maldonado, H., Maricq, M.M., Robinson, A.L., 2014b. Secondary organic aerosol production from diesel vehicle exhaust: impact of aftertreatment, fuel chemistry and driving cycle. Atmos. Chem. Phys. 14, 4643–4659. https://doi.org/10.5194/acp-14-4643-2014.

Hasheminassab, S., Daher, N., Ostro, B.D., Sioutas, C., 2014. Long-term source apportionment of ambient fine particulate matter (PM 2.5) in the Los Angeles Basin: a focus on emissions reduction from vehicular sources. Environ. Pollut. 193, 54–64. https://doi.org/10.1016/j.envpol.2014.06.012.

Heeb, N.V., Forss, A.-M., Brühlmann, S., Lüscher, R., Saxer, C.J., Hug, P., 2006. Three-way catalyst-induced formation of ammonia—velocity- and acceleration-dependent emission factors. Atmos. Environ. 40, 5986–5997. https://doi.org/10.1016/j.atmosenv.2005.12.035.

Ihalainen, M., Tiitta, P., Czech, H., Yli-Pirilä, P., Hartikainen, A., Kortelainen, M.,

Tissari, J., Stengel, B., Sklorz, M., Suhonen, H., Lamberg, H., Leskinen, A., Kiendler-Scharr, A., Harndorf, H., Zimmermann, R., Jokiniemi, J., Sippula, O., 2019. A novel high-volume Photochemical Emission Aging flow tube Reactor (PEAR). Aerosol Sci. Technol. 53, 276–294. https://doi.org/10.1080/02786826.2018.1559918.

Jathar, S.H., Friedman, B., Galang, A.A., Link, M.F., Brophy, P., Volckens, J., Eluri, S., Farmer, D.K., 2017. Linking load, fuel, and emission controls to photochemical production of secondary organic aerosol from a diesel engine. Environ. Sci. Technol. 51, 1377–1386. https://doi.org/10.1021/acs.est.6b04602.

Johnson, T., Caldow, R., Pöcher, A., Mirme, A., Kittelson, D., 2004. A New Electrical Mobility Particle Sizer Spectrometer for Engine Exhaust Particle Measurements. SAE Tech. Papp. 2004–01-1341. https://doi.org/10.4271/2004-01-1341.

Jonson, J.E., Borken-Kleefeld, J., Simpson, D., Nyíri, A., Posch, M., Heyes, C., 2017. Impact of excess NO x emissions from diesel cars on air quality, public health and eutrophication in Europe. Environ. Res. Lett. 12. https://doi.org/10.1088/1748-9326/aa8850.

Kang, E., Root, M.J., Toohey, D.W., Brune, W.H., 2007. Introducing the concept of potential aerosol mass (PAM). Atmos. Chem. Phys. 7, 5727–5744. https://doi.org/10.5194/acp-7-5727-2007.

Karjalainen, P., Pirjola, L., Heikkilä, J., Lähde, T., Tzamkiozis, T., Ntziachristos, L., Keskinen, J., Rönkkö, T., 2014a. Exhaust particles of modern gasoline vehicles: a laboratory and an on-road study. Atmos. Environ. 97, 262–270. https://doi.org/10.1016/j.atmosenv.2014.08.025.

Karjalainen, P., Rönkkö, T., Pirjola, L., Heikkilä, J., Happonen, M., Arnold, F., Rothe, D., Bielaczyc, P., Keskinen, J., 2014b. Sulfur driven nucleation mode formation in diesel exhaust under transient driving conditions. Environ. Sci. Technol. 48, 2336–2343. https://doi.org/10.1021/es405009g.

Karjalainen, P., Timonen, H., Saukko, E., Kuuluvainen, H., Saarikoski, S., Aakko-Saksa, P., Murtonen, T., Bloss, M., Dal Maso, M., Simonen, P., Ahlberg, E., Svenningsson, B., Brune, W.H., Hillamo, R., Keskinen, J., Rönkkö, T., 2016. Time-resolved characterization of primary particle emissions and secondary particle formation from a modern gasoline passenger car. Atmos. Chem. Phys. 16, 8559–8570. https://doi.org/10.5194/acp-16-8559-2016.

Keskinen, J., Pietarinen, K., Lehtimäki, M., 1992. Electrical low pressure impactor. J. Aerosol Sci. 23, 353–360. https://doi.org/10.1016/0021-8502(92)90004-F.

Keskinen, J., Rönkkö, T., 2010. Can real-world diesel exhaust particle size distribution be reproduced in the laboratory? A critical review. J. Air Waste Manag. Assoc. 60, 1245–1255. https://doi.org/10.3155/1047-3289.60.10.1245.

Kittelson, D.B., 1998. Engines and nanoparticles. J. Aerosol Sci. 29, 575–588. https://doi.org/10.1016/S0021-8502(97)10037-4.

Lambe, A.T., Ahern, A.T., Williams, L.R., Slowik, J.G., Wong, J.P.S., Abbatt, J.P.D., Brune, W.H., Ng, N.L., Wright, J.P., Croasdale, D.R., Worsnop, D.R., Davidovits, P., Onasch, T.B., 2011. Characterization of aerosol photooxidation flow reactors: heterogeneous oxidation, secondary organic aerosol formation and cloud condensation nuclei activity measurements. Atmos. Meas. Tech. 4, 445–461. https://doi.org/10.5194/amt-4-445-2011.

Link, M.F., Kim, J., Park, G., Lee, T., Park, T., Babar, Z. Bin, Sung, K., Kim, P., Kang, S., Kim, J.S., Choi, Y., Son, J., Lim, H.J., Farmer, D.K., 2017. Elevated production of NH4NO3from the photochemical processing of vehicle exhaust: implications for air quality in the Seoul Metropolitan Region. Atmos. Environ. 156, 95–101. https://doi.org/10.1016/j.atmosenv.2017.02.031.

Liu, T., Zhou, L., Liu, Q., Lee, B.P., Yao, D., Lu, H., Lyu, X., Guo, H., Chan, C.K., 2019. Secondary organic aerosol formation from urban roadside air in Hong Kong. Environ. Sci. Technol. 53, 3001–3009. https://doi.org/10.1021/acs.est.8b06587.

Malmborg, V.B., Eriksson, A.C., Shen, M., Nilsson, P., Gallo, Y., Waldheim, B., Martinsson, J., Andersson, Ö., Pagels, J., 2017. Evolution of in-cylinder diesel engine soot and emission characteristics investigated with online aerosol mass spectrometry. Environ. Sci. Technol. 51, 1876–1885. https://doi.org/10.1021/acs.est.6b03391.

Mamakos, A., Dardiotis, C., Martini, G., 2012. Assessment of Particle Number Limits for Petrol Vehicles, JRC Scientific and Policy Reports. https://doi.org/10.2788/66205.

Maricq, M.M., Chase, R.E., Xu, N., Podsiadlik, D.H., 2002. The effects of the catalytic converter and fuel sulfur level on motor vehicle particulate matter emissions: gasoline vehicles. Environ. Sci. Technol. 36, 276–282. https://doi.org/10.1021/es010961t.

Mock, P., German, J., Bandivadekar, A., Riemersma, I., 2012. Discrepancies between Type- Approval and " Real-World " Fuel-Consumption and CO2 Values. International Council on Clean Transportation.

Momenimovahed, A., Handford, D., Checkel, M.D., Olfert, J.S., 2015. Particle number emission factors and volatile fraction of particles emitted from on-road gasoline direct injection passenger vehicles. Atmos. Environ. 102, 105–111. https://doi.org/10.1016/j.atmosenv.2014.11.045.

Nordin, E.Z., Eriksson, A.C., Roldin, P., Nilsson, P.T., Carlsson, J.E., Kajos, M.K., Hellén, H., Wittbom, C., Rissler, J., Löndahl, J., Swietlicki, E., Svenningsson, B., Bohgard, M., Kulmala, M., Hallquist, M., Pagels, J.H., 2013. Secondary organic aerosol formation from idling gasoline passenger vehicle emissions investigated in a smog chamber. Atmos. Chem. Phys. 13, 6101–6116. https://doi.org/10.5194/acp-13-6101-2013.

Onasch, T.B., Trimborn, a., Fortner, E.C., Jayne, J.T., Kok, G.L., Williams, L.R., Davidovits, P., Worsnop, D.R., 2012. Soot particle aerosol mass spectrometer: development, validation, and initial application. Aerosol Sci. Technol. 46, 804–817. https://doi.org/10.1080/02786826.2012.663948.

Ortega, A.M., Hayes, P.L., Peng, Z., Palm, B.B., Hu, W., Day, D.A., Li, R., Cubison, M.J., Brune, W.H., Graus, M., Warneke, C., Gilman, J.B., Kuster, W.C., de Gouw, J., Gutiérrez-Montes, C., Jimenez, J.L., 2016. Real-time measurements of secondary organic aerosol formation and aging from ambient air in an oxidation flow reactor in the Los Angeles area. Atmos. Chem. Phys. 16, 7411–7433. https://doi.org/10.5194/acp-16-7411-2016.

Pant, P., Harrison, R.M., 2013. Estimation of the contribution of road traffic emissions to particulate matter concentrations from field measurements: a review. Atmos. Environ. 77, 78–97. https://doi.org/10.1016/j.atmosenv.2013.04.028.

Pérez, N., Pey, J., Cusack, M., Reche, C., Querol, X., Alastuey, A., Viana, M., 2010. Variability of particle number, black carbon, and PM 10 , PM 2.5 , and PM 1 levels and speciation: influence of road traffic emissions on urban air quality. Aerosol Sci. Technol. 44, 487–499. https://doi.org/10.1080/02786821003758286.

Pieber, S.M., Kumar, N.K., Klein, F., Comte, P., Bhattu, D., Dommen, J., Bruns, E.A., Kiluic, D., El Haddad, I., Keller, A., Czerwinski, J., Heeb, N., Baltensperger, U., Slowik, J.G., Prévôt, A.S.H., 2018. Gas-phase composition and secondary organic aerosol formation from standard and particle filter-retrofitted gasoline direct injection vehicles investigated in a batch and flow reactor. Atmos. Chem. Phys. 18, 9929–9954. https://doi.org/10.5194/acp-18-9929-2018.

Platt, S.M., El Haddad, I., Pieber, S.M., Zardini, A.A., Suarez-Bertoa, R., Clairotte, M., Daellenbach, K.R., Huang, R.J., Slowik, J.G., Hellebust, S., Temime-Roussel, B., Marchand, N., De Gouw, J., Jimenez, J.L., Hayes, P.L., Robinson, A.L., Baltensperger, U., Astorga, C., Prévôt, A.S.H., 2017. Gasoline cars produce more carbonaceous particulate matter than modern filter-equipped diesel cars. Sci. Rep. 7, 1–9. https://doi.org/10.1038/s41598-017-03714-9.

Rakowska, A., Wong, K.C., Townsend, T., Chan, K.L., Westerdahl, D., Ng, S., Močnik, G., Drinovec, L., Ning, Z., 2014. Impact of traffic volume and composition on the air quality and pedestrian exposure in urban street canyon. Atmos. Environ 98, 260–270. https://doi.org/10.1016/j.atmosenv.2014.08.073.

Rönkkö, T., Kuuluvainen, H., Karjalainen, P., Keskinen, J., Hillamo, R., Niemi, J.V., Pirjola, L., Timonen, H.J., Saarikoski, S., Saukko, E., Järvinen, A., Silvennoinen, H., Rostedt, A., Olin, M., Yli-Ojanperä, J., Nousiainen, P., Kousa, A., Dal Maso, M., 2017. Traffic is a major source of atmospheric nanocluster aerosol. Proc. Natl. Acad. Sci. 114, 7549–7554. https://doi.org/10.1073/pnas.1700830114.

Rönkkö, T., Virtanen, A., Vaaraslahti, K., Keskinen, J., Pirjola, L., Lappi, M., 2006. Effect of dilution conditions and driving parameters on nucleation mode particles in diesel exhaust: laboratory and on-road study. Atmos. Environ. 40, 2893–2901. https://doi.org/10.1016/j.atmosenv.2006.01.002.

Saha, P.K., Reece, S.M., Grieshop, A.P., 2018. Seasonally varying secondary organic aerosol formation from in-situ oxidation of near-highway air. Environ. Sci. Technol. 52, 7192–7202. https://doi.org/10.1021/acs.est.8b01134.

Saliba, G., Saleh, R., Zhao, Y., Presto, A.A., Lambe, A.T., Frodin, B., Sardar, S., Maldonado, H., Maddox, C., May, A.A., Drozd, G.T., Goldstein, A.H., Russell, L.M., Hagen, F., Robinson, A.L., 2017. Comparison of gasoline direct-injection (GDI) and port fuel injection (PFI) vehicle emissions: emission certification standards, cold-start, secondary organic aerosol formation potential, and potential climate impacts. Environ. Sci. Technol. 51, 6542–6552. https://doi.org/10.1021/acs.est.6b06509.

Simonen, P., Saukko, E., Karjalainen, P., Timonen, H., Bloss, M., Aakko-Saksa, P., Rönkkö, T., Keskinen, J., Dal Maso, M., 2017. A new oxidation flow reactor for measuring secondary aerosol formation of rapidly changing emission sources. Atmos. Meas. Tech. 10, 1519–1537. https://doi.org/10.5194/amt-10-1519-2017.

Suarez-Bertoa, R., Astorga, C., 2016. Isocyanic acid and ammonia in vehicle emissions. Transp. Res. Part D Transp. Environ. 49, 259–270. https://doi.org/10.1016/j.trd.2016.08.039.

Suarez-Bertoa, R., Zardini, A.A., Astorga, C., 2014. Ammonia exhaust emissions from spark ignition vehicles over the New European Driving Cycle. Atmos. Environ. 97, 43–53. https://doi.org/10.1016/j.atmosenv.2014.07.050.

Timonen, H., Karjalainen, P., Saukko, E., Saarikoski, S., Aakko-Saksa, P., Simonen, P., Murtonen, T., Dal Maso, M., Kuuluvainen, H., Bloss, M., Ahlberg, E., Svenningsson, B., Pagels, J., Brune, W.H., Keskinen, J., Worsnop, D.R., Hillamo, R., Rönkkö, T., 2017. Influence of fuel ethanol content on primary emissions and secondary aerosol formation potential for a modern flex-fuel gasoline vehicle. Atmos. Chem. Phys. 17, 5311–5329. https://doi.org/10.5194/acp-17-5311-2017.

Tkacik, D.S., Lambe, A.T., Jathar, S., Li, X., Presto, A.A., Zhao, Y., Blake, D., Meinardi, S., Jayne, J.T., Croteau, P.L., Robinson, A.L., 2014. Secondary organic aerosol formation from in-use motor vehicle emissions using a potential aerosol mass reactor. Environ. Sci. Technol. 48, 11235–11242. https://doi.org/10.1021/es502239v.

Wang, J.M., Jeong, C., Zimmerman, N., Healy, R.M., Hilker, N., Evans, G.J., 2017. Real-world emission of particles from vehicles: volatility and the effects of ambient temperature. Environ. Sci. Technol. 51, 4081–4090. https://doi.org/10.1021/acs.est.6b05328.

Wang, J.M., Jeong, C.H., Zimmerman, N., Healy, R.M., Wang, D.K., Ke, F., Evans, G.J., 2015. Plume-based analysis of vehicle fleet air pollutant emissions and the contribution from high emitters. Atmos. Meas. Tech. 8, 3263–3275. https://doi.org/10.5194/amt-8-3263-2015.

Watne, Å.K., Psichoudaki, M., Ljungström, E., Le Breton, M., Hallquist, M., Jerksjö, M., Fallgren, H., Jutterström, S., Hallquist, Å.M., 2018. Fresh and oxidized emissions from in-use transit buses running on diesel, biodiesel, and CNG. Environ. Sci. Technol. 52, 7720–7728. https://doi.org/10.1021/acs.est.8b01394.

Yli-Ojanperä, J., Kannosto, J., Marjamäki, M., Keskinen, J., 2010. Improving the nanoparticle resolution of the ELPI. Aerosol Air Qual. Res. 10, 360–366. https://doi.org/10.4209/aaqr.2009.10.0060.

Zhao, Y., Lambe, A.T., Saleh, R., Saliba, G., Robinson, A.L., 2018. Secondary organic aerosol production from gasoline vehicle exhaust: effects of engine technology,

cold start, and emission certification standard. Environ. Sci. Technol. 52, 1253–1261. https://doi.org/10.1021/acs.est.7b05045.
Zhao, Y., Saleh, R., Saliba, G., Presto, A.A., Gordon, T.D., Drozd, G.T., Goldstein, A.H., Donahue, N.M., Robinson, A.L., 2017. Reducing secondary organic aerosol formation from gasoline vehicle exhaust. Proc. Natl. Acad. Sci. 114, 6984–6989. https://doi.org/10.1073/pnas.1620911114.
Zhu, R., Hu, J., Bao, X., He, L., Lai, Y., Zu, L., Li, Y., Su, S., 2016. Tailpipe emissions from gasoline direct injection (GDI) and port fuel injection (PFI) vehicles at both low and high ambient temperatures. Environ. Pollut. 216, 223–234. https://doi.org/10.1016/j.envpol.2016.05.066.